Excitation spectrum and supersolidity of a two-leg bosonic ring ladder

Nicolas Victorin,[1] Paolo Pedri,[2] and Anna Minguzzi[1]
[1]*Université Grenoble Alpes, CNRS, LPMMC, 38000 Grenoble, France*
[2]*Laboratoire de Physique des Lasers, CNRS, Université Paris 13, Sorbonne Paris Cité, 99 avenue J.-B. Clément, F-93430 Villetaneuse, France*

(Received 22 October 2019; accepted 22 January 2020; published 26 March 2020)

We consider a system of weakly interacting bosons confined on a planar double lattice ring subjected to two artificial gauge fields. This system is known to display three phases: the Meissner phase, where the flow of particles is carried at the edges of the system without transverse current; a vortex phase, characterized by nonzero transverse current; and a biased-ladder phase, characterized by an imbalance of the population of the two rings. We use the Bogoliubov approximation to determine the excitation spectrum in the three phases, the dynamic structure factor, and the quantum fluctuation corrections to the first-order correlation function. Our analysis reveals supersolid features as well as Josephson modes, corresponding to out-of-phase modes of the finite ring.

DOI: 10.1103/PhysRevA.101.033618

I. INTRODUCTION

Supersolidity is a combined effect of solid order and superfluid flow. In a bosonic system, a supersolid may be formed by breaking two symmetries: (a) the continuous translational symmetry in order to create a crystal order (or discrete translational symmetry on a lattice), and (b) the U(1) symmetry in order to create a Bose-Einstein condensate. The latter is a superfluid thanks to the irrotationality of the velocity field associated with the condensate wave function. The concept of supersolidity was first introduced in the context of liquid helium more than 50 years ago [1,2]. With ultracold atoms, supersolidity has been observed with Bose-Einstein condensates in a cavity [3–5] as well as in dipolar quantum gases [6–9]. Both experimental realizations of supersolidity are based on long-range interactions [10], a key ingredient first introduced by Gross [11]. Another route to reach supersolidity is to have a peculiar single-particle dispersion, e.g., one with two degenerate minima. An example of this second case is provided by spin-orbit coupled Bose gases where supersolidity has also been studied [5,12]. Experimentally, crystal order in spin-orbit coupled Bose gases has been evidenced by the observation of stripes [13]. However, the visibility of the fringes of the density is limited by interspecies interactions and is a major issue to overcome.

In this work, we consider a two-leg bosonic ring lattice subjected to two gauge fields. Here, thanks to the peculiar geometry of the system, the interspecies interactions can be completely suppressed, hence providing a new arena for studying supersolidity in a condition of high fringe visibility. As for the case of a spin-orbit coupled Bose gas, in a two-leg bosonic ring ladder there is no explicit long-range interaction, but it emerges as an effective low-energy property due to the effect of gauge field and tunnel coupling between the rings.

The bosonic ladder under a gauge field in a linear geometry has been the object of intense theoretical work by means of density-matrix renormalization group (DMRG) simulations [14–16] and field-theoretical methods [17–20]. Those studies have provided a complete characterization of the phase diagram of this system, showing various phase. Among them, we mention the chiral superfluid phases, the chiral Mott insulating phases displaying Meissner currents [18,21], and vortex-Mott insulating phases [22]. In the weakly interacting regime, which will be the focus of this work, an additional phase has been predicted [23]: the biased-ladder phase, characterized by an imbalanced population of the bosons between the two legs, explicitly breaking $\mathbb{Z}_2$ symmetry. In conjunction with these theoretical advances, the experimental realization of the bosonic flux ladder has been reported in optical lattices [24] as well as for lattices in synthetic dimensions, both for fermionic and bosonic quantum gases [25,26].

In this paper, we focus on a ladder in the form of a double ring subjected to different flux in each leg. This geometry is amenable to experimental realization and it minimizes the effects of boundaries. For this system, we provide several indications for supersolid features. First of all, we study the properties of the excitation spectrum in order to demonstrate the first-order coherence. In the Meissner phase, we find a single Goldstone mode associated with Bose-Einstein condensation in the only minimum of the single-particle dispersion relation. In the biased ladder phase, in addition to the phonon branch, we predict the existence of a roton minimum. This is the precursor of the vortex phase, in agreement with previous studies [23]. In the vortex phase, two Goldstone modes are observed, associated with the spontaneous breaking of U(1) and translational symmetry. Further proof of the coherence properties of the system is provided by the calculation of the first-order spatial correlation function.

As a second step, we then provide various indications of spatial crystal-like order. First of all, in the excitation spectrum of the vortex phases we find a folding of the Brillouin zone. This is a consequence of the formation of spatial modulations in the mean-field condensate density due to the formation of a vortex lattice along the ring. Furthermore, the analysis of the static structure factor shows the emergence

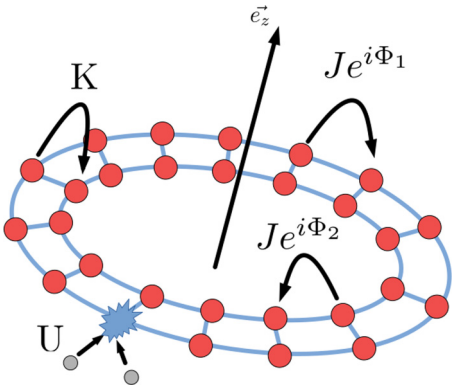

FIG. 1. Sketch of the system studied in this work: coplanar ring lattices with the same number of sites, with interring tunnel energy K, intraring tunnel energies $Je^{i\Phi_p}$ with $p = 1, 2$, and on-site interaction U.

of a peak at finite wave vector, corresponding to the density modulation along the rings.

Taking together the various pieces of evidence on coherence properties and crystalline order, we obtain univocal evidence of supersolidity. Coupled rings under gauge fields hence provide a novel platform for the experimental study of supersolid order with ultracold atoms.

Finally, we address some features peculiar to the finite ring case, and in particular the emergence of Josephson modes for weakly coupled rings. These modes correspond to a spatially uniform out-of-phase oscillation of particles between the rings, hence providing further indication of the coherence among the two rings.

II. MODEL AND METHOD

We consider a Bose gas confined in a double ring lattice (see Fig. 1). In the tight-binding approximation, we model the system using the Bose-Hubbard Hamiltonian:

$$\begin{aligned}\hat{H} &= \hat{H}_0 + \hat{H}_{\text{int}} \\ &= -\sum_{l=1,p=1,2}^{N_s} J_p(\hat{a}^\dagger_{l,p}\hat{a}_{l+1,p}e^{i\Phi_p} + \hat{a}^\dagger_{l+1,p}\hat{a}_{l,p}e^{-i\Phi_p}) \\ &\quad - K\sum_{l=1}^{N_s}(\hat{a}^\dagger_{l,1}\hat{a}_{l,2} + \hat{a}^\dagger_{l,2}\hat{a}_{l,1}) \\ &\quad + \frac{U}{2}\sum_{l=1,p=1,2}^{N_s} a^\dagger_{l,p}\hat{a}^\dagger_{l,p}\hat{a}_{l,p}\hat{a}_{l,p}, \end{aligned} \tag{1}$$

where the position of a particle on each ring is indicated by an integer $l \in [1, N_s]$, with N_s the number of sites in each ring, and $\hat{a}_{l,p}$ and $\hat{a}^\dagger_{l,p}$ are, respectively, the bosonic destruction and creation operators at site l each ring, with $p = 1, 2$ indicating the inner and outer ring, respectively. In Eq. (1), J_1 and J_2 are the tunneling amplitudes from one site to another along each ring, K is the tunneling amplitude between the two rings, connecting only sites with the same position index l, and $\Phi_{1,2}$ are the fluxes threading each ring.

A. Bogoliubov–de Gennes equations

In this work, we focus on the regime of weak interactions and large filling of the double ring. In this regime, the ground state is well approximated by a Bose-Einstein condensate occupying both rings. While there is no Bose-Einstein condensation in an infinite one-dimensional system, in a finite system Bose-Einstein condensation occurs and corresponds to the macroscopic occupation of the lowest energy level of the system. Furthermore, at weak interactions and in a finite-size system, the phase fluctuations typical of low-dimensional systems are weak and cut off by the system size [27].

To obtain the excitation spectrum of the double ring in the Bogoliubov approximation, we start from the Heisenberg equations of motion for the bosonic field operators $\hat{a}_{l,\alpha}$ [28] and we replace $\hat{a}_{l,\alpha}$ in the quantum Hamiltonian (1) by $\hat{a}_{l,\alpha} = \Psi^{(0)}_{l,\alpha} + \delta\hat{a}_{l,\alpha}$. The field $\Psi^{(0)}_{l,\alpha}$ is the ground-state condensate wave function, a solution of the coupled discrete nonlinear Schrödinger equations,

$$\begin{aligned}\mu\Psi_{l,1} &= -J\Psi_{l+1,1}e^{i(\Phi+\phi/2)} - J\Psi_{l-1,1}e^{-i(\Phi+\phi/2)} \\ &\quad - K\Psi_{l,2} + U|\Psi_{l,1}|^2\Psi_{l,1}, \\ \mu\Psi_{l,2} &= -J\Psi_{l+1,2}e^{i(\Phi-\phi/2)} - J\Psi_{l-1,2}e^{-i(\Phi-\phi/2)} \\ &\quad - K\Psi_{l,1} + U|\Psi_{l,2}|^2\Psi_{l,2}, \end{aligned} \tag{2}$$

where $\Phi = \frac{\Phi_1+\Phi_2}{2}$, $\phi = \Phi_1 - \Phi_2$, and μ is the chemical potential. In the following, we will consider for simplicity the case $\Phi = 0$. The next step consists in the expansion and truncation of the Hamiltonian (1) to quadratic order in $\delta\hat{a}_{l,p}, \delta\hat{a}^\dagger_{l,p}$, yielding the Bogoliubov Hamiltonian

$$\hat{H}_{\text{Bog}} = \left(\delta\hat{\mathbf{a}}^\dagger_1, \delta\hat{\mathbf{a}}_1, \delta\hat{\mathbf{a}}^\dagger_2, \delta\hat{\mathbf{a}}_2\right)H^{(2)}\begin{pmatrix}\delta\hat{\mathbf{a}}_1 \\ \delta\hat{\mathbf{a}}^\dagger_1 \\ \delta\hat{\mathbf{a}}_2 \\ \delta\hat{\mathbf{a}}^\dagger_2\end{pmatrix}, \tag{3}$$

where $\delta\hat{\mathbf{a}}^\dagger_p = (\delta\hat{a}^\dagger_{1,p}, \delta\hat{a}^\dagger_{2,p}, \ldots, \delta\hat{a}^\dagger_{l,p})$ and the matrix $H^{(2)}$ can be written in the following form:

$$H^{(2)} = \begin{pmatrix}\mathbf{A}_1 & \mathbf{B}_1 & -\mathbf{K} & 0 \\ \mathbf{B}^*_1 & \mathbf{A}^*_1 & 0 & -\mathbf{K} \\ -\mathbf{K} & 0 & \mathbf{A}_2 & \mathbf{B}_2 \\ 0 & -\mathbf{K} & \mathbf{B}^*_2 & \mathbf{A}^*_2\end{pmatrix}. \tag{4}$$

The matrix $\mathbf{A}_p$ with $p = 1, 2$ is given by

$$\mathbf{A}_p = \begin{pmatrix} 2U|\Psi^{(0)}_{1,p}|^2 & -Je^{i\Phi_p} & \cdots & -Je^{-i\Phi_p} \\ -Je^{-i\Phi_p} & 2U|\Psi^{(0)}_{2,p}|^2 & & \\ \vdots & & \ddots & \vdots \\ -Je^{i\Phi_p} & & \cdots & \begin{matrix} 2U|\Psi^{(0)}_{N_s-1,p}|^2 & -Je^{i\Phi_p} \\ -Je^{-i\Phi_p} & 2U|\Psi^{(0)}_{N_s,p}|^2 \end{matrix} \end{pmatrix}, \tag{5}$$

and $\mathbf{B}_p$ and $\mathbf{K}_p$ are diagonal matrices of dimension $N_s \times N_s$, i.e., $\mathbf{B}_p = \mathrm{diag}(U(\Psi^{(0)}_{1,p})^2, \ldots, U(\Psi^{(0)}_{N_s,p})^2)$, $\mathbf{K} = K\mathbf{I}$, with $\mathbf{I}$ the identity matrix. We search then a transformation to quasiparticle operators $\hat{\gamma}_\nu$ for an excitation in mode ν, such that the Bogoliubov Hamiltonian takes diagonal form

$$H_{\mathrm{Bog}} = \sum_\nu \hbar\omega_\nu \hat{\gamma}^\dagger_\nu \hat{\gamma}_\nu. \tag{6}$$

We use the following general transformation, where the operators $\hat{\gamma}_\nu$ follow the usual bosonic commutation rules, $[\hat{\gamma}_\nu, \hat{\gamma}_{\nu'}] = 0$, $[\hat{\gamma}_\nu, \hat{\gamma}^\dagger_{\nu'}] = \delta_{\nu,\nu'}$,

$$\delta\hat{a}_{l,p} = \sum_\nu h^{(p)}_{\nu,l}\hat{\gamma}_\nu - Q^{*(p)}_{\nu,l}\hat{\gamma}^\dagger_\nu. \tag{7}$$

As a next step, we substitute Eq. (7) into the equation of motion, and we use the following properties:

$$[\hat{\gamma}_\nu, H] = \hbar\omega_\nu\hat{\gamma}_\nu, \tag{8}$$

$$[\hat{\gamma}^\dagger_\nu, H] = -\hbar\omega_\nu\hat{\gamma}^\dagger_\nu. \tag{9}$$

Finally, by equating the coefficients of the different modes $\{h^{(p)}_\nu, Q^{(p)}_\nu\}$ we obtain that the modes have to verify the following eigenvalue problem, corresponding to the Bogoliubov–de Gennes equations for the ring ladder:

$$\omega_\nu \begin{pmatrix} \mathbf{h}^{(1)}_\nu \\ \mathbf{Q}^{(1)}_\nu \\ \mathbf{h}^{(2)}_\nu \\ \mathbf{Q}^{(2)}_\nu \end{pmatrix} = \begin{pmatrix} \mathbf{A}_1 - \mu\mathbf{I} & \mathbf{B}_1 & -\mathbf{K} & 0 \\ -\mathbf{B}^*_1 & -\mathbf{A}^*_1 + \mu\mathbf{I} & 0 & \mathbf{K} \\ -\mathbf{K} & 0 & \mathbf{A}_2 - \mu\mathbf{I} & \mathbf{B}_2 \\ 0 & \mathbf{K} & -\mathbf{B}^*_2 & -\mathbf{A}^*_2 + \mu\mathbf{I} \end{pmatrix} \begin{pmatrix} \mathbf{h}^{(1)}_\nu \\ \mathbf{Q}^{(1)}_\nu \\ \mathbf{h}^{(2)}_\nu \\ \mathbf{Q}^{(2)}_\nu \end{pmatrix}, \tag{10}$$

where $\mathbf{h}^{(p)}_\nu = (h^{(p)}_{\nu,1} \cdots h^{(p)}_{\nu,l} \cdots h^{(p)}_{\nu,N_s})^T$ and $\mathbf{Q}^{(p)}_\nu = (Q^{(p)}_{\nu,1} \cdots Q^{(p)}_{\nu,l} \cdots Q^{(\alpha)}_{\nu,N_s})^T$, and the chemical potential is $\mu = \langle\Psi_{(0)}|H_0|\Psi_{(0)}\rangle + 2\langle\Psi_{(0)}|H_{\mathrm{int}}|\Psi_{(0)}\rangle$. The eigenmodes satisfy the following orthogonality relations, which follow from commutation relations among $\hat{\gamma}_\nu$:

$$\sum_{\nu,p} h^p_{\nu,l}\big(h^{(p)}_{\nu,l'}\big)^* - Q^p_{\nu,l}\big(Q^{(p)}_{\nu,l'}\big)^* = \delta_{l,l'}, \tag{11}$$

$$\sum_{l,p} h^p_{\nu,l}\big(h^{(p)}_{\nu',l}\big)^* - Q^p_{\nu,l}\big(Q^{(p)}_{\nu',l}\big)^* = \delta_{\nu,\nu'}. \tag{12}$$

B. Dynamical structure factor

In this work, we will study the excitation spectrum of the double ring lattice by studying the dynamical structure factor. This is a powerful tool to study correlations in many-body systems both theoretically and experimentally. The dynamical structure factor corresponds to the space and time Fourier transform of the density-density correlation function, and its poles correspond to the collective excitation spectrum of the system.

In the simplest case of a single-component one-dimensional system, the dynamical structure factor is defined as follows [29]:

$$S(q,\omega) = \sum_{s\neq 0} |\langle s|\hat{\rho}_q|0\rangle|^2\delta(\omega - \omega_s), \tag{13}$$

where q and ω are the momentum and energy transferred by the probe to the sample, $|s\rangle$ are many-body eigenstates of the system and $|0\rangle$ is the ground state, $\hat{\rho}_q$ is the density fluctuation operator in momentum space, and $\omega_s = E_s - E_0$ is the energy difference between the excited and the ground state.

For the case of coupled rings, since the excitations belong to both rings, we need to define several dynamical structure factors: $S_{p,p'}(q,\omega)$, with $p, p' = 1, 2$ being the ring index, and

$$S_{p,p'}(q,\omega) = \sum_{s\neq 0} \big|\langle s|\hat{\rho}^{(p,p')}_q|0\rangle\big|^2\delta(\omega - \omega_s) \tag{14}$$

with

$$\hat{\rho}^{(p,p')}_q = \sum_k \hat{a}^\dagger_{k+q,p}\hat{a}_{k,p'}, \tag{15}$$

and q and k are wave vectors corresponding to the longitudinal momentum along each ring, i.e., we have set $\hat{a}_{k,p} = (1/\sqrt{N_s})\sum_j \exp(ikj)\hat{a}_{j,p}$ Using the expansion (7) onto Bogoliubov modes, one can show that in the Bogoliubov approximation, the dynamical structure factors are given by

$$S_{p,p'}(q,\omega) = \sum_{s\neq 0}\left|\sum_l \big(\Psi^{(0)}_{l,p'}h^{*(p)}_{s,l} - \Psi^{*(0)}_{l,p}Q^{*(p')}_{s,l}\big)e^{iql}\right|^2\delta(\omega - \omega_s). \tag{16}$$

To understand the low-energy properties of the system, instead of using the operators $\hat{a}_{k,p}$, it is useful to refer to the operators $\hat{\alpha}_k$ and $\hat{\beta}_k$ that diagonalize the single-particle noninteracting Hamiltonian H_0 [see Appendix A and Eq. (A2) for its definition] and introduce the structure factors $S_{\lambda,\lambda'}$, where $\lambda, \lambda' = \alpha$ or β referring to the corresponding operators. In particular, the low-energy properties of the system under study are governed by the lowest excitation branch associated with the operator $\hat{\beta}_k$, and they can be accessed by studying the dynamical structure factor $S_{\beta,\beta}$:

$$S_{\beta,\beta}(q,\omega) = \sum_{s\neq 0} \big|\langle s|\hat{\rho}^{(\beta)}_q|0\rangle\big|^2\delta(\omega - \omega_s), \tag{17}$$

where we have defined $\hat{\rho}^\beta_q = \sum_k \hat{\beta}^\dagger_{k+q}\hat{\beta}_k$.

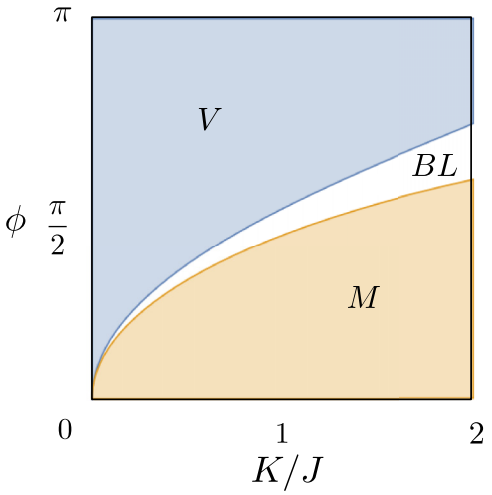

FIG. 2. Phase diagram of the infinite ladder as a function of the flux ϕ per plaquette (dimensionless) and tunnel ratio K/J for interaction strength $Un/J = 0.01$. The Meissner (M), vortex (V), and biased ladder (BL) phases are indicated in the figure.

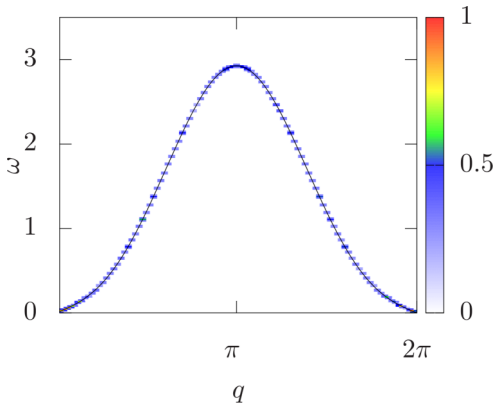

FIG. 3. Excitation spectrum (solid black line) and dynamical structure factor $S_{\beta\beta}$ in the lowest branch basis in the Meissner phase, in the frequency–wave-vector plane (color map, q in units of $1/a$ with a the lattice spacing and ω in units of J) for $Un/J = 0.2$, $\phi = \pi/2$, $K/J = 3$.

C. Static structure factor

Another quantity of interest for the current study is the static structure factor. It yields information on spatial long-range order, e.g., crystal or density wave order, hence it is particularly suited to address the spatial modulations emerging in the vortex phase (see Sec. III below) and to infer supersolidity.

The static structure factor is defined as

$$S_{p,p'}(q) = \sum_s Z_s^{(p,p')}(q), \tag{18}$$

where $Z_s(q) = |\langle s|\rho_q^{(p,p')}|0\rangle|^2$. To access the properties of supersolidity, we need to compute the total static structure factor $S_{\rm tot}(q) = S(q) + S_e(q)$, which takes into account both elastic and inelastic scattering. Inelastic scattering is captured by $S(q)$, and elastic scattering corresponds to the so-called disconnected dynamic structure factor $S_e(q) = Z_{s=0}(q)$ [29].

III. EXCITATION SPECTRUM AS A PROBE OF THE PHASES OF THE TWO-LEG BOSONIC RING LADDER

We proceed in this section to present the results of our calculations of the excitation spectrum of the double ring. As we shall discuss below, we find that the spectrum depends on the specific phase. Before presenting the results in each of the relevant phases for the weakly interacting double ring lattice, we briefly revisit the expected phase diagram.

A. Phase diagram

For the lattice ring at weak interactions, three phases are known: the Meissner (M), vortex (V), and biased-ladder (BL) phases. A schematic phase diagram for the infinite-ladder limit is illustrated in Fig. 2. It is obtained by minimizing the mean-field energy with respect to the ansatz $|\Psi\rangle = \frac{1}{\sqrt{N!}}(\cos(\theta)\hat{\beta}_{k_1}^\dagger + \sin(\theta)\hat{\beta}_{k_2}^\dagger)^N|0\rangle$ [23]. This variational ansatz is known to accurately describe the full mean-field phase diagram, as we checked by comparing it with the full solution of Eqs. (2) [30]. Beyond mean field, various approaches (DMRG, bosonization, renormalization group methods) confirm the existence and stability of the three phases (see, e.g., [16,31]).

The Meissner phase is characterized by vanishing transverse currents $j_{l,\perp} = iK\langle\hat{a}_{l,1}^\dagger\hat{a}_{l,2} - \hat{a}_{l,2}^\dagger\hat{a}_{l,1}\rangle$; the longitudinal currents on each ring, defined as $j_{l,p} = iJ\langle\hat{a}_{l,p}^\dagger\hat{a}_{l+1,p}e^{i\Phi_p} - \hat{a}_{l+1,p}^\dagger\hat{a}_{l,p}e^{-i\Phi_p}\rangle$, are opposite and the chiral current, i.e., $J_c = \sum_l\langle j_{l,1} - j_{l,2}\rangle$, is saturated. The vortex phase is characterized by a modulated density, jumps of the phase of the wave function, and nonzero, oscillating transverse currents that create a vortex pattern. The biased-ladder phase has only longitudinal currents as in the Meissner phase, but displays an imbalanced population between the two rings.

B. Excitation spectrum in the Meissner phase

In the Meissner phase, the ground-state solution for the condensate wave function is uniform in space and corresponds to a condensate occupying the $k = 0$ state. The lowest branch of the spectrum shows a single phononic mode close to $k = 0$. This is the Goldstone mode associated with the spontaneous breaking of the U(1) symmetry. Notice that even though we solve two equations for the condensate wave functions on each ring [see Eqs. (2) and (10)], only the global phase is free to fluctuate while the relative phase is fixed by the tunnel coupling among the two rings. A simplified expression for the dispersion relation of this branch can be obtained by performing the Bogoliubov approximation on the lower branch of the single-particle spectrum [23]. It reads

$$\epsilon_k^M = \tfrac{1}{2}\sqrt{(Un + 2\tilde{\epsilon}_k)^2 - (2Unu_kv_k)^2} \tag{19}$$

with $\tilde{\epsilon}_k = E_-(k) - E_-(0)$ and u_k, v_k defined in Appendix A. An analytical solution of the full two-band problem is provided in Appendix B.

Figure 3 shows the dynamical structure factor as obtained by the numerical diagonalization of the Bogoliubov–de Gennes equations. The poles of the dynamical structure factor in the frequency–wave-vector plane are in excellent agreement with Eq. (19), also shown in the figure.

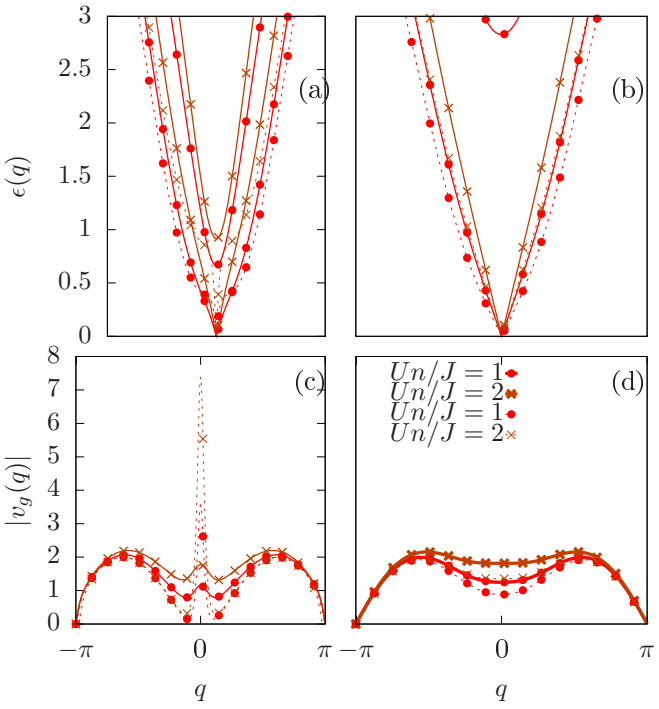

FIG. 4. Upper panels: dispersion relations $\epsilon(q)$ (in units of J) as a function of wave vector q (in units of $1/a$) in the Meissner phase for (a) $\phi = \pi/4$, $K/J = 0.1$ and (b) $\phi = \pi/4$, $K/J = 1$ for various values of the interaction strength indicated in panel (d) (lines with symbols). Bottom panels: corresponding group velocity (in units of Ja) as a function of wave-vector q (in units of $1/a$) for (c) $\phi = \pi/4$, $K/J = 0.1$ and (d) $\phi = \pi/4$, $K/J = 1$. The solid lines with symbols correspond to the Meissner excitation spectrum taking into account both the lower and upper branch of the noninteracting problem [see Eq. (B2)], while the dashed lines with symbols correspond to the lowest band approximation [see Eq. (19)].

The dispersion relation ϵ_k obtained from the full solution [Eq. (B2)] and the corresponding group velocity $v_g = \partial\epsilon_k/\partial k$ is shown in Fig. 4 for various values of the interaction strength. The main effect of the coupling at strong interactions is to change the sound velocity, to decrease the region where the spectrum is linear and modify the shape of the dispersion at finite momenta, where the group velocity displays a minimum.

C. Excitation spectrum in the biased-ladder phase

In the biased-ladder phase, as well as in the vortex phase, the single-particle dispersion relation has two minima at $k = k_1, k_2$. In the biased-ladder phase, only one of the two minima is macroscopically populated. The excitation spectrum (see Fig. 5) shows a phononic Goldstone mode and a rotonic structure [23]. A similar behavior is found in spin-orbit coupled Bose gases [32]. At fixed flux ϕ, when decreasing the coupling K between the ring, the vortex phase is accessed through a softening of the roton minimum. The system enters the vortex phase when the roton minimum decreases down to a critical (nonzero) value, thus indicating a first-order transition, similarly to what was predicted for dipolar gases [33].

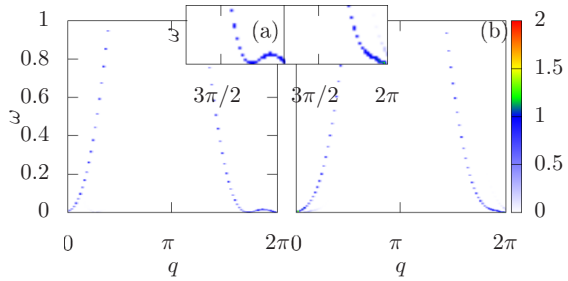

FIG. 5. Dynamical structure factor in the frequency–wave-vector plane (ω in units of J and q in units of $1/a$) for the biased-ladder phase, (a) for the case $Un/J = 0.01$ and $K/J = 1.15$, (b) for the case $Un/J = 0.05$ and $K/J = 1.4$. The insets show a zoom of the same figures at small frequency and for $qa \simeq 2\pi$. In all panels, $N_s = 100$, $\phi = \pi/2$.

D. Excitation spectrum in the vortex phase

At the mean-field level, the vortex phase is characterized by a macroscopic occupation of a superposition state involving two single-particle momentum modes $k = k_1, k_2$ corresponding to the minima of the single-particle dispersion relation [23]. This gives rise to a spatial modulation in the density profile with wave vector $k_v = k_1 - k_2$. This is not a finite-size effect: in the noninteracting limit, one can easily check that the amplitude of the modulation does not depend on the system size (see, e.g., [30]), and we have numerically checked that this is also the case in the presence of interactions.

The numerical result for the dynamical structure factor $S_{\beta,\beta}(q,\omega)$ in the vortex phase is shown in Fig. 6. We find various minima of the dispersion relation for $q = 0$ and $q = k_2 - k_1$ as well as at the points $q = 2\pi$ and $q = 2\pi$

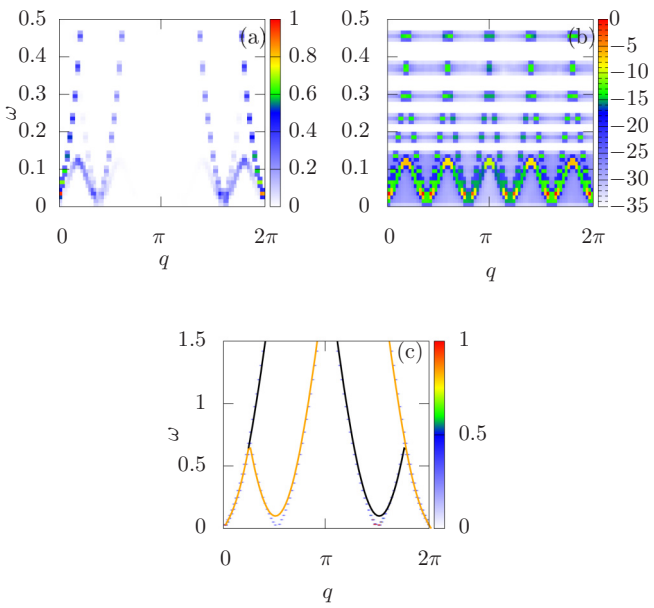

FIG. 6. Dynamical structure factor $S_{\beta\beta}(q,\omega)$ in the frequency–wave-vector plane (ω in units of J and q in units of $1/a$) in the vortex phase for $K/J = 0.8$ in linear (a) and logarithmic (b) scale; (c) dynamical structure factor $S_{\beta\beta}(q,\omega)$ for $K/J = 0$. The other parameters for all the panels are $\phi = \pi/2$, $Un/J = 0.2$, $N_s = 80$.

$-(k_2-k_1)$. Two linear dispersion branches are found around each of these minima, characterized by two different sound velocities. These branches correspond to the two Goldstone modes associated with the breaking of U(1) and spatial translational symmetry, and hence they may be viewed as phase modes and crystal modes [34–36].

An analysis of the dynamical structure factor in log scale [see Fig. 6(b)] shows a folding of the Brillouin zone for the excitations, corresponding to the underlying ground-state vortex superlattice felt by the Bogoliubov excitations. Specifically, for the parameters chosen in the calculation of Fig. 6 we have that the ground-state density profile has a modulation with wave vector k_1-k_2, leading to a $\frac{2\pi}{k_1-k_2}$-times folding of the excitation spectrum, i.e., 5-times in the case of Fig. 6.

The overall features of the excitation spectrum can be understood by comparing it with the one in the $K=0$ case. In this regime, the rings are independent and the excitation spectrum is given by two branches, obtained by solving the Bogoliubov equations for each ring separately:

$$\epsilon_k^{V(1)} = -\tfrac{1}{2}(\epsilon_{k+k_1}-\epsilon_{k-k_1} \pm \sqrt{(\epsilon_{k+k_1}+\epsilon_{k-k_1})^2+4U|\psi_0|^2(\epsilon_{k+k_1}+\epsilon_{k-k_1})}),$$
$$\epsilon_k^{V(2)} = -\tfrac{1}{2}(\epsilon_{k+k_2}-\epsilon_{k-k_2} \pm \sqrt{(\epsilon_{k+k_2}+\epsilon_{k-k_2})^2+4U|\psi_0|^2(\epsilon_{k+k_2}+\epsilon_{k-k_2})}), \quad (20)$$

where $\epsilon_k = 2J[1-\cos(k)]$.

Exploiting a low-energy model (see Appendix C), we can then understand qualitatively the behavior of the excitation spectrum at small but finite K. In this regime, the excitations can tunnel from one ring to the other with k-dependent interaction parameters $\tilde{U}$ and $\tilde{\tilde{U}}$ (see Appendix C). These scattering events break the degeneracy of the sound velocities around each minimum. In Fig. 7 we show the various dynamical structure factors $S_{p,p'}(q,\omega)$ in the ring basis. All the excitation branches observed in $S_{\beta\beta}(q,\omega)$ are visible, with variable spectral weight depending on the choice of p, p'. The off-diagonal dynamical structure factors show the symmetry relation $S_{12}(q,\omega)=S_{21}(q,-\omega)$.

E. Experimental probe of the dynamical structure factor

In ultracold atomic gases, the dynamical structure factor can be measured using two-photon optical Bragg spectroscopy [37], according to the following scheme: two laser beams are impinged upon the condensate, the difference in the wave vectors of the beams defines the momentum transfer $\hbar q$, and the frequency difference defines the energy transfer $\hbar\omega$ to the fluid. Both values of q and ω can be tuned by changing the angle between the two beams and varying the frequency difference of the two laser beams. Several experiments have reported the observation of the dynamical structure factor with ultracold atoms (see, e.g., Refs. [9,38–40]).

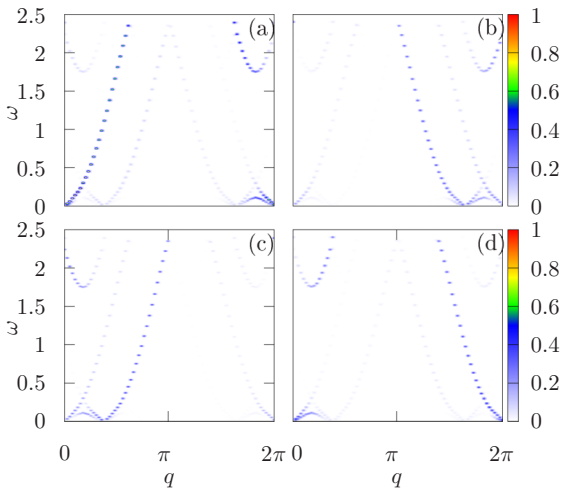

FIG. 7. Dynamical structure factor $S_{p,p'}(q,\omega)$ in the frequency–wave-vector plane (ω in units of J and q in units of $1/a$) in the ring basis with $p,p'=1,2$ in the vortex phase: (a) $S_{1,1}(q,\omega)$, (b) $S_{1,2}(q,\omega)$, (c) $S_{2,1}(q,\omega)$, and (d) $S_{2,2}(q,\omega)$. For all panels we have taken $\phi=\pi/2$, $N_s=80$, $K/J=0.8$, and $Un/J=0.2$.

A way of probing the excitation spectrum of the double ring studied in this work is to use angular momentum spectroscopy [41]: in this case, one needs two laser beams denoted by 1,2 in high-order Laguerre-Gauss modes with optical angular momenta $l_{1,2}$ and frequencies $\omega_{1,2}$. Their corresponding electric fields read $E_{1,2}(r)=f_{l_1,l_2}(r)e^{-il_{1,2}\theta-i\omega_{1,2}t}$, where the radial mode functions $f_l(r)\propto(r/r_0)^{|l|}e^{r^2/2r_0^2}$ need to be chosen in order to match the shape of the double ring to probe.

IV. SUPERSOLIDITY

Supersolidity is characterized by both superfluidity and spatial long-range order. In the presence of a Bose-Einstein condensate, superfluidity is ensured by the phase coherence of the condensate. First-order coherence is quantified by the spatial decay of the one-body density matrix. Spatial order can be probed through the study of the static structure factor. In this section, we will use the excitation eigenmodes obtained from the Bogoliubov–de Gennes equations to evaluate both quantities and conclude about supersolidity of the double ring ladder.

A. Coherence properties: One-body density matrix

To study the coherence properties of the system, we consider the one-body density matrix $\rho^{(1)}_{\alpha,\alpha'}(j,l)=\langle\hat{a}^\dagger_{j,\alpha}\hat{a}_{l,\alpha'}\rangle$, which in the Bogoliubov approximation reads [42,43]

$$\rho^{(1)}_{p,p'}(j,l)=\sqrt{\rho^{(0)}_{j,p}\rho^{(0)}_{l,p'}}\exp\left(-\frac{1}{2}\sum_s\left|\frac{\mathcal{Q}^{(p)}_{s,j}}{|\Psi^{(0)}_{j,p}|}-\frac{\mathcal{Q}^{(p')}_{s,l}}{|\Psi^{(0)}_{l,p'}|}\right|^2\right), \quad (21)$$

where the function in the exponential relates to the fluctuation of the phase of the condensate, and $\rho^{(0)}_{l,p}$ stands for the

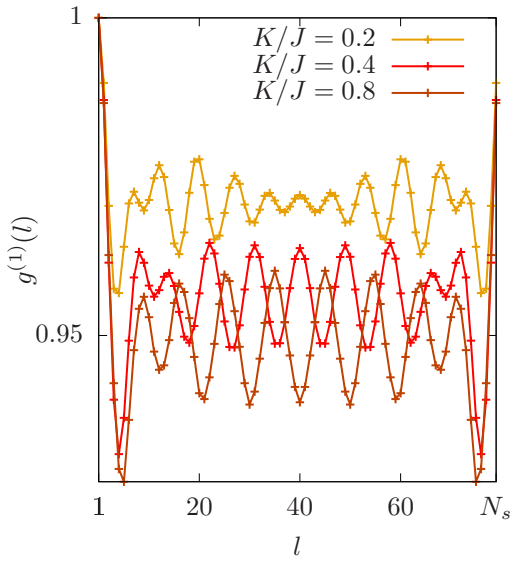

FIG. 8. Averated first-order correlation function $g^{(1)}_{(1,1)}(l)$ (dimensionless) as a function of the site index l (dimensionless) for the inner ring in the vortex phase for increasing values K/J from top to bottom, as indicated in the figure. The other parameters are $\phi = \pi/2$, $N_s = 80$, and $Un/J = 0.2$.

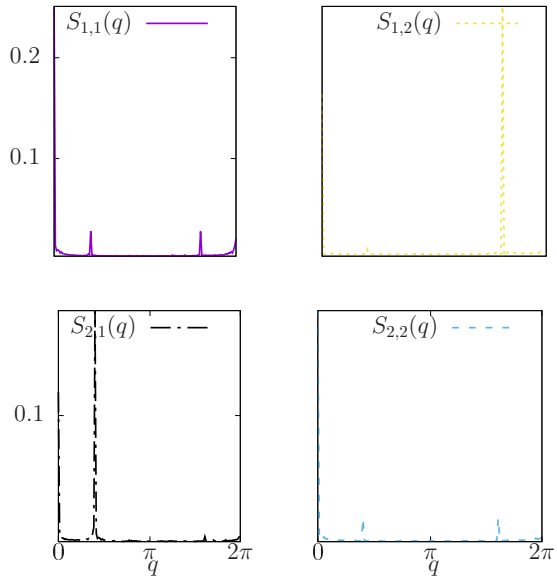

FIG. 9. Total static structure factors $S_{p,p'}(q)$ (dimensionless) as a function of wave vector q (in units of $1/a$) with $p, p' = 1, 2$ as indicated in the panels, for $\phi = \pi/2$, $N_s = 150$, $K/J = 0.8$, and $Un/J = 0.2$.

mean-field ground-state density profile of each ring. Since in the vortex phase the system is inhomogeneous, the one-body density matrix does not depend only on the coordinate difference $j - l$. Therefore, to estimate the coherence we study the averaged first-order correlation function defined as

$$g^{(1)}_{(p,p')}(l) = \sum_j \rho^{(1)}_{(p,p')}(j, j+l)/\sqrt{\rho_{j,p}\rho_{j+l,p'}}. \tag{22}$$

Figure 8 shows the $g^{(1)}$ correlations in the vortex phase along the inner ring. As the coupling K/J between the rings increases, we notice that the correlations in the ring decrease. However, even for large values of K/J, the coherence in the vortex phase stays high even at large distances. This corresponds to a large condensate fraction, thereby implying Bose-Einstein condensation (BEC) and superfluidity.

B. Spatial order: Static structure factor

To probe the spatial crystalline order expected in the vortex phase, we compute the total static structure factor $S_{\rm tot}(k)$ (see Sec. II C), corresponding to the sum of the elastic contribution coming from the density profile, and the inelastic contribution coming from the density fluctuations. The resulting static structure factor is illustrated in Fig. 9. We clearly see a peak at wave vectors $k = k_2 - k_1$ and $k = 2\pi - (k_2 - k_1)$, revealing the crystalline order associated with the spatial modulations of the condensate density profile. Putting together this result with the results of Sec. IV A above, we conclude that the bosons in the vortex phase of the ring ladder display supersolid features.

V. SMALL-RING LIMIT AND NATURE OF THE EXCITATIONS

We report in this section a study of the nature of the excitations in the different phases of the system, highlighting in particular the peculiar aspects related to the finite size of the ring. For this purpose, we calculate the density fluctuations $\delta n^{\nu}_{l,p}$ defined as $\langle s|\rho_{l,p}|0\rangle$, which can be obtained from the Bogoliubov eigenmodes $h^{(p)}_{\nu,l}$ and $Q^{(p)}_{\nu,l}$ according to

$$\delta n^{\nu}_{l,p} = 2\,\mathrm{Re}\big[\Psi^{(0)}_{l,p}\big(h^{(p)}_{\nu,l}\big)^* - \big(\Psi^{(0)}_{l,p}\big)^* Q^{(p)}_{\nu,l}\big]. \tag{23}$$

Our results for the density fluctuations of the chosen low-energy modes are shown in Fig. 10. Among the various types of excitation modes, in addition to the phononic Goldstone

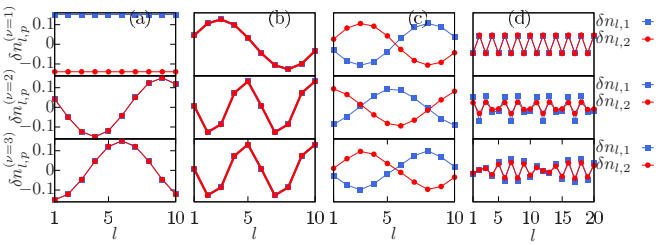

FIG. 10. Excitation eigenmodes $\delta n_{l,p}$ (dimensionless) as a function of the position l along each ring (dimensionless, blue lines with squares $p = 1$, red lines with circles $p = 2$) for the first three excited Bogoliubov modes. (a) Josephson out-of-phase mode and two in-phase phonon modes in the Meissner phase for $N_s = 10$, $K/J = 0.1$, $\phi = 0.1$, $Un/J = 0.1$; (b) in-phase phonon modes in the Meissner phase for $N_s = 10$, $K/J = 0.8$, $\phi = 0.1$, $Un/J = 0.2$; (c) out-of-phase mode in the vortex phase for $N_s = 10$, $K/J = 0.01$, $\phi = \pi/4$, $Un/J = 0.2$; (d) in-phase modes in the biased-ladder phase with $N_s = 20$, $K/J = 1$, and $\phi = \pi/2$.

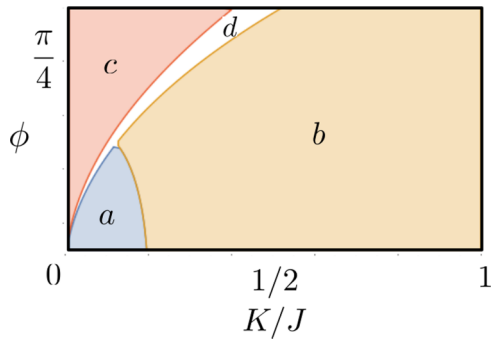

FIG. 11. Sketch of the phase diagram in the (ϕ, K) plane, with ϕ dimensionless and K in units of J, at fixed interaction strength $Un/J = 0.2$ and $N_s = 10$ as deduced from the analysis of the excitation eigenmodes, summarizing the cases illustrated in Fig. 10. The colored regions marked by letters indicate (a) Meissner phase with the lowest mode of Josephson type, (b) Meissner phase with the lowest mode of charge type, (c) Vortex phase with the lowest mode of spin type, and (d) biased-ladder phase with the lowest mode of charge type.

modes propagating along each ring, we identify the Josephson mode, typical of a finite ring system, which is characterized by spatially homogeneous density fluctuations and out-of-phase oscillations of the relative populations among the two rings, as in the small-amplitude dynamics of the Josephson effect [44,45].

We see in Fig. 10 that a uniform Josephson mode occurs at low energy in the Meissner phase for low enough coupling among the rings, whereas higher excited mode are of phonons of charge (i.e., in-phase) type. Close to the phase boundary, in the vortex phase we find that the lowest excitation is a spin (i.e., out-of-phase) oscillation. In the nearby Meissner phase, the lowest excitation becomes phonon excitation of charge type, as well as in the biased-ladder phase.

The Josephson modes are found in the Meissner phase for weak tunnel coupling K/J and weak flux ϕ. To estimate the parameter regime where phonon or Josephson modes are present in the ring, we provide here some estimates based on energy scales. In the Meissner phase, close to $k \to 0$ the spectrum has a linear behavior,

$$\epsilon_k^M \approx E_{\rm ph} k, \tag{24}$$

where

$$E_{\rm ph} = \frac{2\pi J^2}{K N_s} \sqrt{\frac{U}{J}\left[\frac{K^2}{J^2}\cos(\phi/2) + \left(\frac{U}{J} - \frac{2K}{J}\right)\sin(\phi/2)^2\right]}. \tag{25}$$

When comparing it to the energy of the Josephson mode, which scales as the band gap between the upper and lower branch of the excitation spectrum $E_{\rm gap} \approx K$, we predict that the region where Josephson modes are allowed, i.e., when $E_{\rm gap} < E_{\rm ph}$, appears at very low K and ϕ (see Fig. 11). This is in agreement with the numerical solution of the Bogoliubov equations. Moreover, we obtain that the Josephson region shrinks upon increasing the number of sites in the ring, thereby showing that the Josephson modes are a finite-size effect.

VI. CONCLUSIONS

In conclusion, in this work we have performed a detailed study of the excitation spectrum of a weakly interacting Bose gas in a two-leg bosonic ring ladder subjected to two artificial gauge fields. For all three phases expected at weak interactions, i.e., the Meissner, vortex, and biased-ladder phase, we have solved the Bogoliubov–de Gennes equations for the ring ladder and calculated the dynamical structure factor. For a cigar-shaped gas and for a one-dimensional gas in a linear atomic waveguide, the dynamical structure factor has already been experimentally measured. Here we propose that it is accessed in the ring geometry by angular momentum spectroscopy.

Our main predictions are a single-phonon-like dispersion at long wavelength in the Meissner phase, a roton minimum emerging in the biased-ladder phase, and two phononic branches in the vortex phase. Furthermore, we find evidence of the underlying spatially modulated structure of the vortex phase in the spectrum by a folding of the Brillouin zone of the excitations.

Using the Bogoliubov excitation eigenmodes, we have also calculated the first-order correlation function, monitoring the coherence of the gas, and we found that it remains high all over the rings. This feature, together with the diagonal long-range order in the vortex phase, is a hallmark of the supersolid nature of the fluid. The emergence of supersolidity in this system is quite remarkable as, contrary to the spin-orbit coupled Bose gas, the visibility of the fringes can be tuned thanks to the absence of interspecies contact interactions in the current model. Finally, we have shown the emergence of Josephson excitations in a finite ring, corresponding to population imbalance oscillations among the two rings.

It would be interesting to study the excitation spectrum at larger interaction strengths, where the nature of the ground state changes on a fragmented condensate [46] or a fragmented Fermi sphere [47] at intermediate and large interactions, respectively. Also, it would be interesting to confirm the supersolid nature beyond the mean-field and Bogoliubov approximations, where the spatial modulations in the density profile are expected to be washed out by the quantum fluctuations, but spatial order should persist in the density-density correlations and in the static structure factor [19,20]. The knowledge of the excitation spectrum is also useful for atomtronics applications [48], e.g., for the study of transport in the linear-response regime, when two leads are attached to the ring [49–51].

ACKNOWLEDGMENTS

We thank L. Amico, R. Citro, and S. Moroni for stimulating discussions. We acknowledge funding from the ANR SuperRing (Grant No. ANR-15-CE30-0012).

APPENDIX A: NONINTERACTING REGIME

We first proceed by analyzing the noninteracting problem. The diagonalization of H_0 yields the following two-band

Hamiltonian:

$$\hat{H}_0 = \sum_k \hat{\alpha}_k^\dagger \hat{\alpha}_k E_+(k) + \hat{\beta}_k^\dagger \hat{\beta}_k E_-(k), \tag{A1}$$

where

$$\begin{pmatrix} \hat{a}_{k,1} \\ \hat{a}_{k,2} \end{pmatrix} = \begin{pmatrix} v_k & u_k \\ -u_k & v_k \end{pmatrix} \begin{pmatrix} \hat{\alpha}_k \\ \hat{\beta}_k \end{pmatrix}, \tag{A2}$$

where functions u_k and v_k depend on the parameter ϕ and K/J, and they are given here for simplicity in the case $\Phi = 0$ treated in this work,

$$v_k = \sqrt{\frac{1}{2}\left(1 + \frac{\sin(\phi/2)\sin(k)}{\sqrt{(K/2J)^2 + \sin^2(\phi/2)\sin^2(k)}}\right)}, \tag{A3}$$

$$u_k = \sqrt{\frac{1}{2}\left(1 - \frac{\sin(\phi/2)\sin(k)}{\sqrt{(K/2J)^2 + \sin^2(\phi/2)\sin^2(k)}}\right)}. \tag{A4}$$

The momentum in units of inverse lattice spacing takes discrete values given by $k = \frac{2\pi n}{N_s}$, with $n = 0, 1, 2, \ldots, N_s - 1$, and the dispersion relation $E_\pm$ reads

$$E_\pm(k) = -2J\cos(\phi/2)\cos(k) \pm \sqrt{K^2 + (2J)^2 \sin(\phi/2)^2 \sin(k)^2}. \tag{A5}$$

APPENDIX B: EXCITATION SPECTRUM IN THE MEISSNER PHASE

In the Meissner phase, the mean-field solution is uniform in space so that $\Psi_{l,p} = \sqrt{N/2N_s} = \sqrt{n}$. The equation of motion for the Bogoliubov modes is expanded in plane-wave solutions $h_{\nu,l}^{(p)} = h_q^{(p)} e^{iql}$, $Q_{\nu,l}^{(p)} = Q_q^{(p)} e^{iql}$, where ν is identified as the plane-wave momentum q longitudinal to the rings. It reads

$$\epsilon(q)\begin{pmatrix} h_q^{(1)} \\ Q_q^{(1)} \\ h_q^{(2)} \\ Q_q^{(2)} \end{pmatrix} = \begin{pmatrix} \epsilon_+(q) + Un & -Un & -K & 0 \\ Un & -\epsilon_-(q) - Un & 0 & K \\ -K & 0 & \epsilon_-(q) + Un & -Un \\ 0 & K & Un & -\epsilon_+(q) + Un \end{pmatrix} \begin{pmatrix} h_q^{(1)} \\ Q_q^{(1)} \\ h_q^{(2)} \\ Q_q^{(2)} \end{pmatrix}, \tag{B1}$$

where $\epsilon_\pm(q) = -2J[\cos(k \pm \phi/2) - \cos(\phi/2)] + K$.

This matrix is diagonalizable and the positive eigenvalues read

$$\epsilon(q) = \frac{1}{\sqrt{2}}\{\epsilon_+^2 + \epsilon_-^2 + 2(\epsilon_+ + \epsilon_-)Un + 2K^2 \pm \sqrt{(\epsilon_+^2 - \epsilon_-^2)^2 + 4Un(\epsilon_+^3 + \epsilon_-^3 - \epsilon_-^2\epsilon_+ + \epsilon_+^2\epsilon_-) + 4K^2[(\epsilon_+ + \epsilon_-)^2 + 4Un(\epsilon_+ + \epsilon_- + Un)]}\}^{1/2}. \tag{B2}$$

For a similar derivation, see Ref. [52].

APPENDIX C: BOGOLIUBOV EXCITATION SPECTRUM FOR THE LOWEST SINGLE-PARTICLE BRANCH

In this part, using the following ansatz:

$$|\Psi\rangle = \frac{1}{\sqrt{N!}}\left(\hat{\beta}_{k_1}^\dagger e^{-i\psi_1} + \hat{\beta}_{k_2}^\dagger e^{-i\psi_2}\right)^N |0\rangle \tag{C1}$$

for the ground state, we study the excitation spectrum of the vortex phase by analyzing the Bogoliubov excitations on top of the lowest single-particle excitation branch β. The contributions from the upper branch, which corresponds to particles created by the operators $\hat{\alpha}_k$, are negligible when the interaction strength is much smaller than the gap among the lower and upper branch of the single-particle spectrum.

To perform the Bogoliubov analysis, we start from the original Hamiltonian (1) and compute the interacting part of the Hamiltonian in the free-particle diagonal basis $\{\beta_k^\dagger, \beta_k\}$ (see [17]). We obtain

$$\hat{H}_{\text{int}} = \frac{U}{2N_s}\sum_{q,k,r} K(k-q, r+q, k, r)\hat{\beta}_{k-q}^\dagger \hat{\beta}_{r+q}^\dagger \hat{\beta}_k \hat{\beta}_r, \tag{C2}$$

where the kernel K is given by $K(q_1, q_2, q_3, q_4) = u_{q_1}u_{q_2}u_{q_3}u_{q_4} + v_{q_1}v_{q_2}v_{q_3}v_{q_4}$.

Here we see that the restriction to the lowest branch yields a one-dimensional Bose gas with effective nonzero range interaction potential. We then proceed by performing the Bogoliubov approximation: we assume that the states k_1 and k_2 are macroscopically occupied and so we approximate the operators in those states by $\mathbb{C}$-numbers:

$$\beta_{k_1} = \sqrt{N_0/2}e^{i\psi_1}, \tag{C3}$$

$$\beta_{k_2} = \sqrt{N_0/2}e^{i\psi_2}, \tag{C4}$$

where N_0 is the number of condensed particles in the whole system. We then rewrite the Hamiltonian keeping up all terms up to quadratic order in operators $\hat{\beta}_{k\neq k_1,k_2}$, $\hat{\beta}_{k\neq k_1,k_2}^\dagger$. To conserve the particle number within the Bogoliubov approximation, we write the number of condensed particles as a function of the total particle number using the relation $N_0 = N - \sum_{k\neq(k_1,k_2)}\hat{\beta}_k^\dagger\hat{\beta}_k$. This procedure yields the following quadratic Hamiltonian:

$$\hat{H} = E^{(0)} + \hat{H}_{\text{Bog}}, \tag{C5}$$

where $H^{(0)}$ is the mean-field energy in the vortex phase given by

$$E^{(0)} = NE_-(k_1) + \frac{UNn}{4}\left[1 + 2u_{k_1}^2 v_{k_1}^2\right],$$

$$\hat{H}_{\text{Bog}} = \sum_{k\neq(k_1,k_2)} \tilde{\epsilon}_k \hat{\beta}_k^\dagger \hat{\beta}_k + \sum_k \hat{\beta}_{2k_1+k}^\dagger \hat{\beta}_{-k}^\dagger U_{1,k} + \text{H.c.}$$

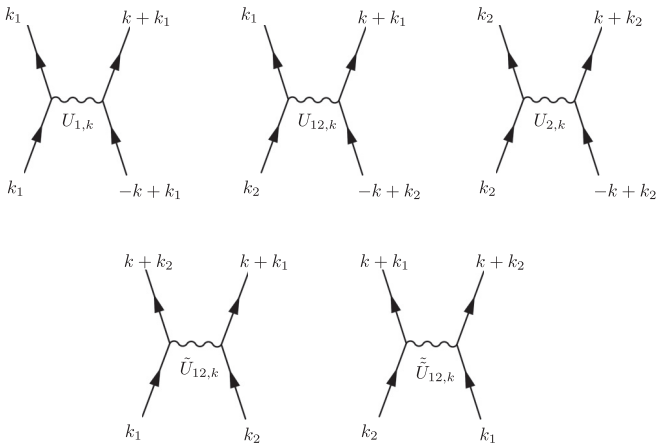

FIG. 12. Scheme depicting the main collision channels for the effective interactions among particles belonging to the lower branch of the single-particle excitation spectrum.

$$+\sum_k \hat{\beta}^\dagger_{2k_2+k}\hat{\beta}^\dagger_{-k}U_{2,k} + \text{H.c.} + \sum_k \hat{\beta}^\dagger_{k_1+k_2+k}\hat{\beta}^\dagger_{-k}U_{12,k}$$
$$+ \text{H.c.} + \sum_k \hat{\beta}^\dagger_{k_1-k_2+k}\hat{\beta}_k(\tilde{U}_{12,k} + \text{c.c.})$$
$$+\sum_k \hat{\beta}^\dagger_{k_2-k_1+k}\hat{\beta}_k(\tilde{\tilde{U}}_{12,k} + \text{c.c.}) \tag{C6}$$

and the coefficients $\tilde{\epsilon}_k$ and U_k correspond to the Feynman diagrams of Fig. 12 and read

$$\tilde{\epsilon}_k = E_-(k) - E_-(k_1) - \frac{UN}{2N_s}\left(1 + 2u^2_{k_1}v^2_{k_1}\right)$$
$$+ \frac{UN}{N_s}\left(u^2_{k_1}u^2_k + v^2_{k_1}v^2_k\right) + \frac{UN}{N_s}\left(u^2_{k_2}u^2_k + v^2_{k_2}v^2_k\right), \tag{C7}$$
$$U_{1,k} = \frac{UN}{4N_s}K(k_1, k_1, 2k_1 + k, -k), \tag{C8}$$
$$U_{2,k} = \frac{UN}{4N_s}K(k_2, k_2, 2k_2 + k, -k), \tag{C9}$$
$$U_{12,k} = \frac{UN}{4N_s}2K(k_1 + k_2 + k, -k, k_1, k_2), \tag{C10}$$
$$\tilde{U}_{12,k} = \frac{2UN}{N_s}K(k_1, k_2, k_1 - k_2 + k, k), \tag{C11}$$
$$\tilde{\tilde{U}}_{12,k} = \frac{2UN}{N_s}K(k_1, k_2, k_2 - k_1 + k, k). \tag{C12}$$

APPENDIX D: DYNAMICAL STRUCTURE FACTOR OF THE NONINTERACTING CASE AND FULL EXPRESSION IN THE BOGOLIUBOV APPROXIMATION

By taking the ground state as $|0\rangle = \frac{1}{\sqrt{2}}(|k_1\rangle + |k_2\rangle)$, the dynamical structure factor readily reads

$$S_{\beta,\beta}(q, w) = \tfrac{1}{2}[\delta(\omega - \omega_{q+k_1}) + \delta(\omega - \omega_{q+k_2})] \tag{D1}$$

with $\omega_k = E_-(k) - E_-(k_1)$. We see that it consists of two bands that correspond only for $k_1 = k_2 = 0$ (Meissner phase) or $k_1 = -k_2 = -\pi$.

Using Eq. (7) and Eq. (16), the dynamical structure factor in the Bogoliubov approximation reads

$$S_{\beta,\beta}(q, \omega)$$
$$= \sum_{s\neq 0}\Big|\sum_k u_{k+q}u_k\left(\left(\tilde{h}^{(1)}_{s,k+q}\right)^*\tilde{\Psi}^{(0)}_{k,1} - \left(\tilde{\Psi}^{(0)}_{k+q,1}\tilde{Q}^{(1)}_{s,-k}\right)^*\right)$$
$$+ v_{k+q}v_k\left(\left(\tilde{h}^{(2)}_{s,k+q}\right)^*\tilde{\Psi}^{(0)}_{k,2} - \left(\tilde{\Psi}^{(0)}_{k+q,2}\tilde{Q}^{(2)}_{s,-k}\right)^*\right)$$
$$+ u_{k+q}v_k\left(\left(\tilde{h}^{(1)}_{s,k+q}\right)^*\tilde{\Psi}^{(0)}_{k,2} - \left(\tilde{\Psi}^{(0)}_{k+q,1}\tilde{Q}^{(2)}_{s,-k}\right)^*\right)$$
$$+ v_{k+q}u_k\left(\left(\tilde{h}^{(2)}_{s,k+q}\right)^*\tilde{\Psi}^{(0)}_{k,1} - \left(\tilde{\Psi}^{(0)}_{k+q,2}\tilde{Q}^{(1)}_{s,-k}\right)^*\right)|^2\delta(\omega - \omega_s), \tag{D2}$$

where $\tilde{h}_{s,k}$, $\tilde{Q}_{s,k}$, and $\tilde{\Psi}^{(0)}_{k,\alpha}$ are the Fourier transforms of $h^{(\alpha)}_{\nu,l}$, $Q^{(\alpha)}_{\nu,\alpha}$ of the excitation and of the condensate wave function $\Psi^{(0)}_{l,\alpha}$, respectively.

[1] A. J. Leggett, Phys. Rev. Lett. **25**, 1543 (1970).
[2] G. V. Chester, Phys. Rev. A **2**, 256 (1970).
[3] B. Kristian, G. Christine, B. Ferdinand, and E. Tilman, Nature (London) **464**, 1301 (2010).
[4] J. Léonard, A. Morales, P. Zupancic, T. Esslinger, and T. Donner, Nature (London) **543**, 87 (2017).
[5] J.-R. Li *et al.*, Nature (London) **543**, 91 (2017).
[6] F. Böttcher, J. N. Schmidt, M. Wenzel, J. Hertkorn, M. Guo, T. Langen, and T. Pfau, Phys. Rev. X **9**, 011051 (2019).
[7] L. Tanzi, E. Lucioni, F. Famà, J. Catani, A. Fioretti, C. Gabbanini, R. N. Bisset, L. Santos, and G. Modugno, Phys. Rev. Lett. **122**, 130405 (2019).
[8] L. Chomaz, D. Petter, P. Ilzhöfer, G. Natale, A. Trautmann, C. Politi, G. Durastante, R. M. W. van Bijnen, A. Patscheider, M. Sohmen, M. J. Mark, and F. Ferlaino, Phys. Rev. X **9**, 021012 (2019).
[9] G. Natale, R. M. W. van Bijnen, A. Patscheider, D. Petter, M. J. Mark, L. Chomaz, and F. Ferlaino, Phys. Rev. Lett. **123**, 050402 (2019).
[10] L. Renate *et al.*, Nature (London) **532**, 476 (2016).
[11] E. P. Gross, Phys. Rev. **106**, 161 (1957).
[12] Y. Li, G. I. Martone, L. P. Pitaevskii, and S. Stringari, Phys. Rev. Lett. **110**, 235302 (2013).
[13] W. Ketterle and N. J. van Druten, Phys. Rev. A **54**, 656 (1996).
[14] M. Piraud, F. Heidrich-Meisner, I. P. McCulloch, S. Greschner, T. Vekua, and U. Schollwock, Phys. Rev. B **91**, 140406(R) (2015).
[15] M. Di Dio, S. De Palo, E. Orignac, R. Citro, and M. L. Chiofalo, Phys. Rev. B **92**, 060506(R) (2015).
[16] E. Orignac *et al.*, New J. Phys. **18**, 055017 (2016).
[17] A. Tokuno and A. Georges, New J. Phys. **16**, 073005 (2014).

[18] E. Orignac and T. Giamarchi, Phys. Rev. B **64**, 144515 (2001).
[19] E. Orignac, R. Citro, M. Di Dio, and S. De Palo, Phys. Rev. B **96**, 014518 (2017).
[20] R. Citro, S. De Palo, M. Di Dio, and E. Orignac, Phys. Rev. B **97**, 174523 (2018).
[21] A. Dhar, T. Mishra, M. Maji, R. V. Pai, S. Mukerjee, and A. Paramekanti, Phys. Rev. B **87**, 174501 (2013).
[22] A. Petrescu and K. Le Hur, Phys. Rev. Lett. **111**, 150601 (2013).
[23] R. Wei and E. J. Mueller, Phys. Rev. A **89**, 063617 (2014).
[24] M. Atala *et al.*, Nat. Phys. **10**, 588 (2014).
[25] B. K. Stuhl *et al.*, Science **349**, 1514 (2015).
[26] M. Mancini *et al.*, Science **349**, 1510 (2015).
[27] D. S. Petrov, G. V. Shlyapnikov, and J. T. M. Walraven, Phys. Rev. Lett. **85**, 3745 (2000).
[28] A. L. Fetter, Ann. Phys. **70**, 67 (1972).
[29] F. Zambelli, L. Pitaevskii, D. M. Stamper-Kurn, and S. Stringari, Phys. Rev. A **61**, 063608 (2000).
[30] N. Victorin, F. Hekking, and A. Minguzzi, Phys. Rev. A **98**, 053626 (2018).
[31] S. Uchino and A. Tokuno, Phys. Rev. A **92**, 013625 (2015).
[32] G. I. Martone, Y. Li, L. P. Pitaevskii, and S. Stringari, Phys. Rev. A **86**, 063621 (2012).
[33] A. Minguzzi, N. H. March, and M. P. Tosi, Phys. Rev. A **70**, 025601 (2004).
[34] S. Saccani, S. Moroni, and M. Boninsegni, Phys. Rev. Lett. **108**, 175301 (2012).
[35] T. Macrì, F. Maucher, F. Cinti, and T. Pohl, Phys. Rev. A **87**, 061602(R) (2013).
[36] S. M. Roccuzzo and F. Ancilotto, Phys. Rev. A **99**, 041601(R) (2019).
[37] A. Brunello, F. Dalfovo, L. Pitaevskii, S. Stringari, and F. Zambelli, Phys. Rev. A **64**, 063614 (2001).
[38] D. M. Stamper-Kurn, A. P. Chikkatur, A. Görlitz, S. Inouye, S. Gupta, D. E. Pritchard, and W. Ketterle, Phys. Rev. Lett. **83**, 2876 (1999).
[39] R. Landig *et al.*, Nat. Commun. **6**, 7046 (2015).
[40] N. Fabbri, M. Panfil, D. Clément, L. Fallani, M. Inguscio, C. Fort, and J.-S. Caux, Phys. Rev. A **91**, 043617 (2015).
[41] N. Goldman, J. Beugnon, and F. Gerbier, Phys. Rev. Lett. **108**, 255303 (2012).
[42] Y. Castin and R. Dum, Phys. Rev. Lett. **77**, 5315 (1996).
[43] L. Fontanesi, M. Wouters, and V. Savona, Phys. Rev. Lett. **103**, 030403 (2009).
[44] A. Burchianti, C. Fort, and M. Modugno, Phys. Rev. A **95**, 023627 (2017).
[45] G.-S. Paraoanu, S. Kohler, F. Sols, and A. J. Leggett, J. Phys. B, **34**, 4689 (2001).
[46] A. R. Kolovsky, Phys. Rev. A **95**, 033622 (2017).
[47] N. Victorin, T. Haug, L. C. Kwek, L. Amico, and A. Minguzzi, Phys. Rev. A **99**, 033616 (2019).
[48] L. Amico, G. Birkl, M. Boshier, and L.-C. Kwek, New J. Phys. **19**, 020201 (2017).
[49] R. Fazio, F. W. J. Hekking, and A. A. Odintsov, Phys. Rev. Lett. **74**, 1843 (1995).
[50] A. Tokuno, M. Oshikawa, and E. Demler, Phys. Rev. Lett. **100**, 140402 (2008).
[51] T. Haug, R. Dumke, L.-C. Kwek, and L. Amico, Quantum Sci. Technol. **4**, 045001 (2019).
[52] A. Keleş and M.Ö. Oktel, Phys. Rev. A **91**, 013629 (2015).